Biomed Microdevices
DOI 10.1007/s10544-009-9287-7

Controlled cellular orientation on PLGA microfibers with defined diameters

C. M. Hwang · Y. Park · J. Y. Park · K. Lee · K. Sun · A. Khademhosseini · S. H. Lee

Abstracts In this study, we investigated the effects of the diameter of microfibers on the orientation (angle between cells' major axis and the substrate fiber long axis) of adhered cells. For this purpose, mouse fibroblast L929 cells were cultured on the surface of PLGA fibers of defined diameters ranging from 10 to 242 μm, and their adhesion and alignment was quantitatively analyzed. It was found that the mean orientation of cells and the spatial variation of cell alignment angle directly related to the microfiber diameter. Cells that were cultured on microfibrous scaffolds oriented along the long axis of the microfiber and the orientation increased as the fiber diameter decreased. For the fiber diameter of 10 μm, the mean orientation was 3.0± 0.2° (mean±SE), whereas for a diameter of 242 μm, it decreased to 37.7±2.1°. Using these studies we demonstrate that fibroblasts have a characteristic alignment on microscale fibers and that the microscale fiber diameter plays a critical role in cellular orientation. The ability to control cellular alignment on engineered tissue scaffold can be a potentially powerful approach to recreate the microscale architecture of engineered tissues. This may be important for engineering a variety of human tissues such as tendon, muscle and nerves as well as applications in 3D tissue culture and drug screening.

Keywords PLGA fibers · Fibroblasts · Scaffold · Cell orientation · Focal contact

C. M. Hwang · J. Y. Park · K. Lee · S. H. Lee (✉)
Department of Biomedical Engineering,
College of Health Science, Korea University,
Jeongneung-dong, Seongbuk-gu,
Seoul 136-703, Republic of Korea
e-mail: dbiomed@korea.ac.kr

C. M. Hwang · Y. Park · K. Sun
Korea Artificial Organ Center, Korea University,
Anam-dong 5ga, Seongbuk-gu,
Seoul 136-705, Republic of Korea

C. M. Hwang · A. Khademhosseini
Center for Biomedical Engineering, Department of Medicine,
Brigham and Women's Hospital, Harvard Medical School,
65 Landsdowne Street,
Cambridge, MA 02139, USA

C. M. Hwang · A. Khademhosseini
Harvard-MIT Division of Health Sciences and Technology,
Massachusetts Institute of Technology,
Cambridge, MA 02139, USA

Y. Park · K. Sun
Department of Biomedical Engineering, College of Medicine,
Korea University,
Seoul 136-705, Republic of Korea

Published online: 26 February 2009

1 Introduction

Recently many biological studies have revealed that cellular decisions such as adhesion, proliferation, migration, differentiation and apoptosis are affected by the surrounding microenvironmental cues such as biochemical, mechanical and topological signals. Therefore, understanding of a cell's interactions with its microenvironment has become a key goal in medical and biological studies. To date, many studies have been carried out on the effect of biochemical and mechanical factors on cells. Another important cue is the topology of extracellular molecules, however, for years less attention was paid to the topological effects because the fabrication of *in vivo*-like micro- or nano-topology has been difficult. Recently, microfabrication technology has been applied as a powerful tool in

manipulating the surface microarchitecture from micro- to nanometer length scales(Khademhosseini et al. 2006). Microengineering technology can be used to fabricate micro- and nano-structures of defined shapes, periodicity, and sizes, to study the effects of topography on cellular behavior(Teixeira et al. 2003; Monsees et al. 2005; Choi et al. 2007). So far, many of these approaches have been carried out on two-dimensional (2-D) surfaces, which do not necessarily correlate to the response in three-dimensional (3-D) environments. In the body, cells are exposed to a 3-D environments which signals the cells about whether it should proliferate, differentiate, migrate or remain quiescent. Therefore, conventional 2-D patterns or micropatterned 3-D structures (like grooves) have limitations in mimicking the *in vivo* environments for tissue culture(Yamamoto et al. 2007) or drug screening.(Mai et al. 2007) Many components of the natural extracellular matrix (ECM) have a fibrous structure (L'Heureux et al. 2006); thus the ability to understand cellular behavior on fibers would provide new opportunities in tissue formation and regeneration by enabling closer control of cell shape, adhesion and differentiation.

A number of previous studies have aimed to analyze cell alignment on fibrous substrates (Neumann et al. 2003; Lee et al. 2005; Smeal et al. 2005; Bashur et al. 2006; Murugan and Ramakrishna 2007; Chew et al. 2008; Tian et al. 2008). These reports have observed cell alignment along the fibers. However, many observations were performed on small diameter fibers such as nanofibers that were fabricated by electrospinning (Lee et al. 2005; Murugan and Ramakrishna 2007; Chew et al. 2008; Tian et al. 2008), relative to only few studies on individual microfibers (Neumann et al. 2003; Smeal et al. 2005; Bashur et al. 2006). Therefore the ability to engineer biodegradable fibers of defined diameters can be used to systematically study these observations to determine the effects of fiber size on cell alignment.

In this paper, we used a microfluidic-based fiber generation process to investigate the topographical effect (especially 3D-curved structures) of microfibers on the guided cell alignment. For this purpose, we cultured cells on micro-scale PLGA fibers and quantitatively analyzed the correlation between the cell alignment and fiber diameter. To produce size controlled (diameters from 10 to 242 um) PLGA microfibers, a microfluidic chip system was used to fabricate and align the fibers unidirectionally. Subsequently, we studied the alignment of mouse fibroblasts (Wong et al. 2007) that are known to change shape and orientation on textured surfaces (Dunn and Heath 1976; Ohara and Buck 1979). Morphologies of cells cultured on the PLGA microfibers were analyzed and the micro-environmental control of cell orientation was investigated.

2 Materials and Methods

2.1 Materials

PLGA (Resomer RG 504H, 50:50) random copolymer was purchased from Boehringer Ingelheim. This polymer has an intrinsic viscosity of 0.45~0.65 dL/g in 0.1% $CHCl_3$ solution in room temperature. Polydimethylsiloxane (PDMS, Sylgard 184) was obtained from Dow Corning and dimethyl sulfoxide (DMSO, purity 99%), glutaraldehyde (25% aqueous solution), glycerol anhydrous (purity 98%), osmium tetroxide (OsO_4) and *t*-butyl alcohol (purity 98%) were purchased from Samchun (Korea).

For cell culture, phosphate buffered saline (PBS) and Dulbecco's Modified Eagle Medium (DMEM) were purchased from Gibco Laboratories and fetal bovine serum (FBS) was obtained from BD science. For immunostaining, Alexa Fluor 568 phalloidin, 4',6-diamidine-2'-phenylindole, dihydrochloride (DAPI), mouse IgG anti-vinculin and Prolong Gold antifade reagent were purchased from Invitrogen (USA).

2.2 PLGA fiber preparation

PLGA fibers were prepared by microfluidic wet spinning system. This microfiber fabrication process is reported previously for fiber, microsphere and microcapsule generation with UV curable polymers (Jeong et al. 2004, 2005; Kim et al. 2005; Oh et al. 2006). In brief, this system is composed of a pulled glass tube inserted into the PDMS block with feeding tube connected both glass tube and syringe pumps as shown in Fig. 1(a). Core solution was 10% (*w*/*v*) PLGA solution dissolved in DMSO and sheath solution was 50% (v/v) glycerin in water solution. Parallel-aligned fiber samples were prepared by winding PLGA fibers around 14×14 mm cover glasses fixed on a rotating DC motor axis (Hwang et al. 2008). After winding, the fiber wound cover glasses were rinsed twice with deionized water (DW) for 4 h each for further removal of DMSO. Finally, microfiber specimens were immersed in 1.0% glutaraldehyde solution for 4 h for sterilization and then rinsed three times with PBS for at least 1 h and then stored in 4°C refrigerator before cell culture. All the fibrous PLGA samples were used within 5 days after fabrication.

2.3 Cell culture

Mouse fibroblasts of L929 cell line were used in this study. Before cell seeding, PLGA fibers were rinsed twice with fresh PBS for 5 min each and immersed cell culture media in each well of a 12-well plate. After removal of the culture medium, 50 μL of cell suspension containing 1×10^5 cells was gently loaded on each microfiber, incubated for 1 h for

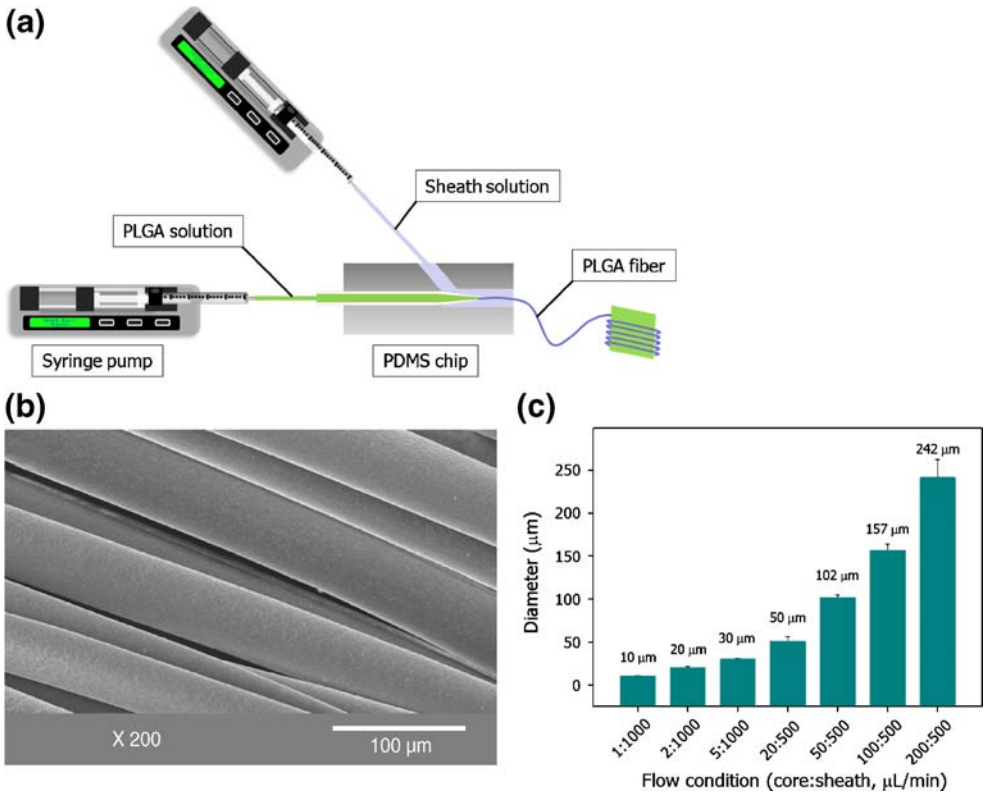

Fig. 1 (**a**) The microfluidic fiber spinning system with glass tube, PDMS block and two syringe pumps and winding around a cover glass. Core solution is 10% (*w*/*v*) PLGA polymer in DMSO and sheath solution is 50% glycerin in water. (**b**) SEM image of PLGA fibers produced by microfluidic wet spinning system. (**c**) Microfluidically spun PLGA fiber diameter with different flow condition with 30 μm tip diameter (n=20, mean±SD)

attachment of cells and then 2 mL of the culture medium was added. We used DMEM containing 4.5 g/L D-glucose, L-glutamine and 110 mg/L sodium pyruvate with 10% heat inactivated fetal bovine serum (FBS), penicillin (100 units/mL), and streptomycin sulfate (100 μg/mL) as the cell culture media. Medium was changed 1 day after seeding. After 3 days culture, the samples were fixed for scanning electron microscopy (SEM) analysis and immunostained for confocal scanning laser microscope investigation.

2.4 Immunocytochemistry of L929 fibroblasts

To analyze the formation of focal contacts and actin filament arrangements, F-actin and vinculin were immunologically labeled with fluorescent dyes. Cells were gently rinsed with PBS, fixed with 4% paraformaldehyde solution for 1 h under 37°C, and then permeabilized with 1% triton X-100 in PBS solution. Blocking was achieved by using 3% (*w*/*v*) bovine serum albumin (BSA) in PBS solution for 30 min. Alexa Fluor 568 phalloidin (1:40) and mouse IgG antivinculin (1:200) were diluted in PBS including 1% BSA and reacted for 1 h. Secondary antibody was reacted to primary vinculin antibody for another 1 h. During the nuclear staining stage, DAPI stock solution (1 mg/mL) was diluted in DI water (1:1,000) and reacted for 5 min. Finally, to preserve fluorescence, samples were coated with antifade reagent and observed with confocal laser scanning microscope (Carl-Zeiss LSM 5).

2.5 Scanning electron microscopy

The scaffolds were washed with PBS to remove non-adherent cells and then fixed with 2.5% glutaraldehyde for 2 h at room temperature. After rinsing twice with PBS for 5 min, samples were treated with a 1% osmium tetroxide (OsO_4) solution for 60 min and then dehydrated through a series of graded ethanol washes from 50% to 100% for 20 min each and then freeze-dried with Maxi-Dry Lyo (Heto Holten, Denmark). The cell cultured scaffolds were then sputter-coated with platinum at a pressure of 100 mTorr for 6 min. A field emission scanning electron microscope (FE-SEM; Hitachi, S4700, Japan) was used to investigate the cell alignment on the PLGA scaffolds.

2.6 Measurement of cell orientation

SEM images were used to quantify the orientation of L929 fibroblasts on the surface of PGLA fibers. SEM images were analyzed with AxioVision LE 4.5 software. The 3-D cell and fiber configurations were 'projected' into 2-D SEM images. An illustration of the relative parameters of cells on the PLGA fiber is shown in Fig. 2.Cell orientation θ was

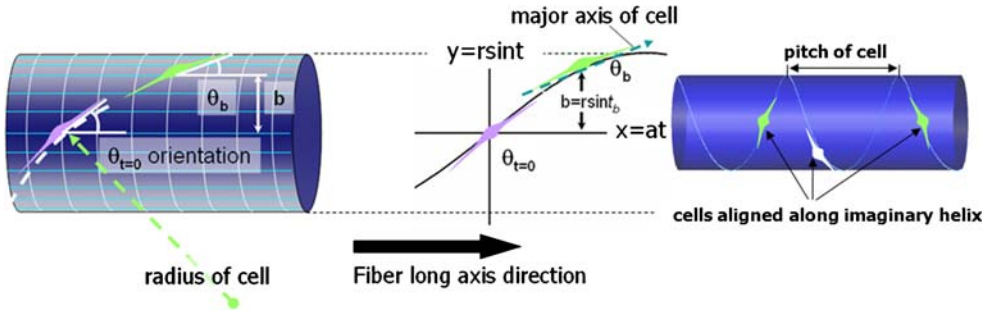

Fig. 2 Schematic of parameters used for quantification for cell alignment on the surface of fiber scaffolds. The measured values are projected cell length, cell width, cell area, alignment angle θ_b, radius r and distance b fiber from fiber long axis. Cell alignment angles were converted to orientation $\theta_{t=0}$ and radius of cells. Projected images of cells having same helix curve parameters $\theta_{t=0}$, identical orientation

defined as the angle between the major axis of a cell and long axis of PGLA fibers. The measured projected values are cell alignment angle θ_b, distance b from the fiber major axis to measurement position of a cell, cell area, cell width and length of a cell (schematic in Fig. 2 and SEM images in Fig. 3). When the major axis of a cell does not cross the centerline of PLGA fiber, cell alignment angle θ_b was measured by creating a line parallel to the fiber long axis crossing the cell center as shown in Fig. 2. By assuming the cells were aligned along the imaginary helical line on the fiber surface, the orientation angle of a cell was calculated from helix equations (Weisstein 2008).

When a cell measured angle θ_b at distance b from the center line of fiber radius r, cell orientation $\theta_{t=0}$ at the center line of a fiber is,

$$\theta_{t=0} = \tan^{-1}\left[\frac{\tan\,\theta_b}{\cos\left(\sin^{-1}\left(\frac{b}{r}\right)\right)}\right] \tag{1}$$

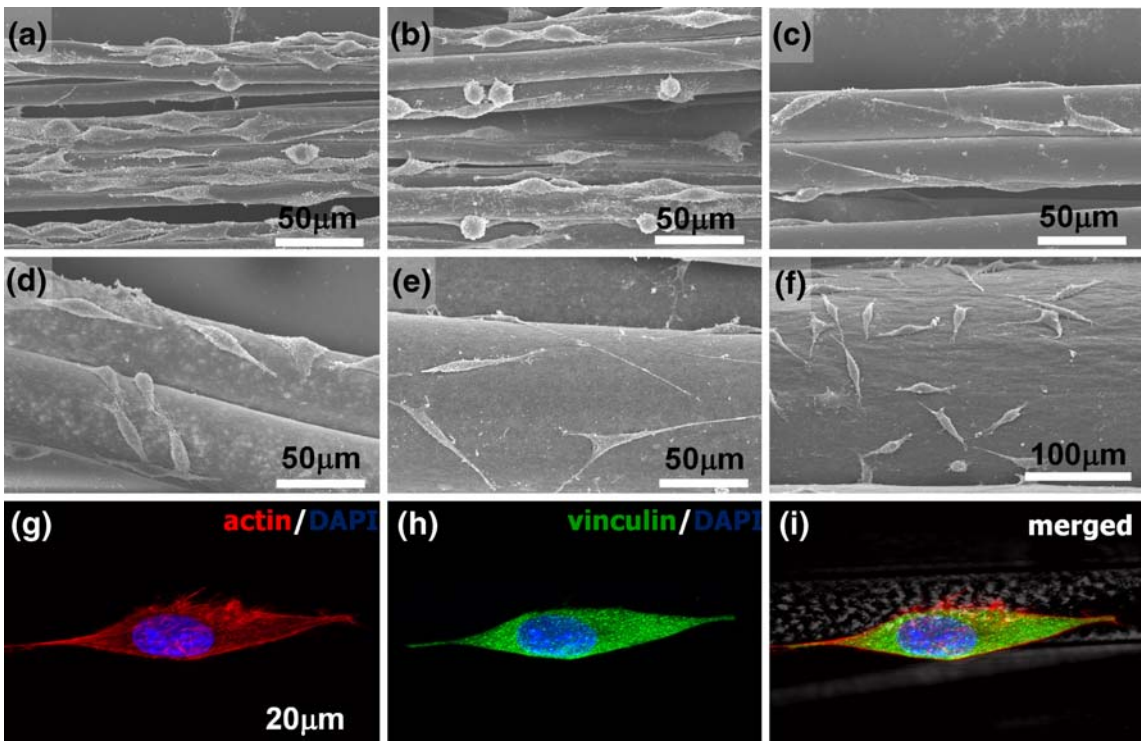

Fig. 3 Cell morphology of mouse L929 fibroblasts on different diameter PLGA fibers shows different orientations with respect to the long axis of fibers. PLGA fiber diameters are (**a**) 10 μm, (**b**) 20 μm, (**c**) 30 μm, (**d**) 50 μm, (e) 102 μm, (**f**) 242 μm, (**g**–**i**) immunostained cell on the PLGA fiber with 30 μm diameter. *Blue region* in (**i**) is DAPI stained nuclei. *Dashed lines* in (**g**) indicate the boundary of PLGA fiber

And the curvature of a cell τ is (Smeal et al. 2005; Weisstein 2008),

$$\tau = \frac{\sin^{-2}\ \theta_{t=0}}{r} \tag{2}$$

And radius of a cell is 1/τ, and pitch of a cell assumed as a helix is 2πa,

$$\tau = \frac{r}{\tan\ \theta_{t=0}} \tag{3}$$

3 Results and discussion

3.1 PLGA Fiber morphology

During microfluidic wet spinning, we controlled the core polymer solution flow rate from 1 to 200 μL/min and the sheath flow rate from 500 to 1,000 μL/min. Magnified images of the PLGA fibers are shown in Fig. 1(b). The fibers had relatively smooth surfaces and were highly aligned. Using a glass pipette tip with 30 μm inner diameter for microfiber spinning, we obtained PLGA fibers with mean diameters of 10, 20, 30, 50, 102, 157 and 242 μm with high uniformity (Fig. 1(c)). These results indicate that the microfluidic device can produce PLGA microfiber with flexible size range in a simple and cost effective manner (Hwang et al. 2008).

3.2 Cell alignment on the PLGA microfibers

The changes in the morphologies of adherent L929 cells on the PLGA fibers are shown in Fig. 3. Without any ECM pre-coating (e.g.: fibronectin, laminin) before cell seeding, L929 cells adhered and proliferated on the surface of the fibers after 3 days. As shown in Fig. 3, cells also aligned differently as a function of PLGA microfiber diameter after 3 days of culture. In Fig. 4(a), the cell orientation graph shows that the cell orientation decreases as the diameter of PLGA microfiber increases. As the fiber diameter increases, the angle between the cell and the major axis of PLGA fiber deviates from the parallel direction, and the spatial deviation of cell orientation increases with the substrate fiber diameter as shown in Fig. 4(b). When the mean fiber diameter is 10 μm, the orientation was 3.0±0.2° (mean± SE) and increased to 37.7±2.1° (mean±SE) when the fiber diameter is 242 μm. As a control, the orientation of cells cultured on the planar culture dish was analyzed to show that their mean angle was approximately 45° (data not shown) which means that their direction is random to any measurement reference axis. Fig. 4(a), (b) illustrates that the cellular deviation to fiber axis increases with fiber size and shows that cell properties on large diameter substrates start resembling those of cells on planar surfaces.

Figure 5 shows the results from measured values about the projected data of cells on the different sized fibers such as cell area, cell long axis and aspect ratio of cells (ratio of cell length and cell width). The projected cell area increases with the fiber substrate diameter. As shown in Fig. 5(a), the projected cell area increases with fiber diameter in the small diameter region ($p<0.01$), but somewhat decreased at large fiber sizes from 157 to 242 μm ($p<0.05$). The measured cell length and aspect ratio showed different characteristic from cell area. There does not appear to be a significant difference between 20 and 30 μm data in cell area, length and aspect ratio of cells in Fig. 5. Between 20 and 30 μm fiber diameter region, cells show minimum aspect ratio whereas the cell length has maximum values.

There are interesting aspects in 20 to 30 μm diameter results. Independently measured values of the cell length, orientation and cell area show local minimum or maximum values in this region. In this region, the cell area did not change significantly but the cell length was significantly higher than other conditions as shown in Fig. 5(a), (b). Also independently calculated curvature of cells in Fig. 4(c) peaks in this region which cell radii and helix pitches in Fig. 6(a) and Fig. 6(b) show minimum values in this region.

To date, a number of studies has been carried out to study cell alignment on modified substrates. For example, Bashur et al. reported that fibroblasts cultured on electro-spun PLGA nano-fiber mesh exhibited cell morphologies that correlated with fiber diameter and fiber orientation (Bashur et al. 2006). It is also reported that in these conditions cells aligned along the nano- and microfibers with diameters ranging from 500 nm to 10 μm and the number and length of adhered cell were increased as the fiber diameter decrease (Tian et al. 2008). On grooved surfaces, Bettinger et al. examined the alignment of endothelial cells on patterns with round cross-section and reported that cells oriented along the substrate patterns as spacing decreased from 5 to 2.5 μm (Bettinger et al. 2006). On the cylindrical substrates, cultured nerve cells on filamentous substrates and reported that substrate curvature influenced the direction of nerve outgrowth (Smeal et al. 2005). However, to our knowledge there has not been a systematic study that analyzed the effects of microfiber diameter in the range of ten to hundreds of micrometers.

The significance of the present study is that the fibroblast cell orientation showed controllable change by defining the diameter of fiber PLGA fibers. This is different from neurite extension under similar condition (Smeal et al. 2005), and also different from the PLGA nano-, micro-fibers with smaller diameters (Tian et al. 2008). When nerve cells were cultured on the fiber substrates, the mean direction of neurite outgrowth aligned with the direction of minimum curvature (fiber's long axis; Smeal et al. 2005), which means the axon orientations did not change with

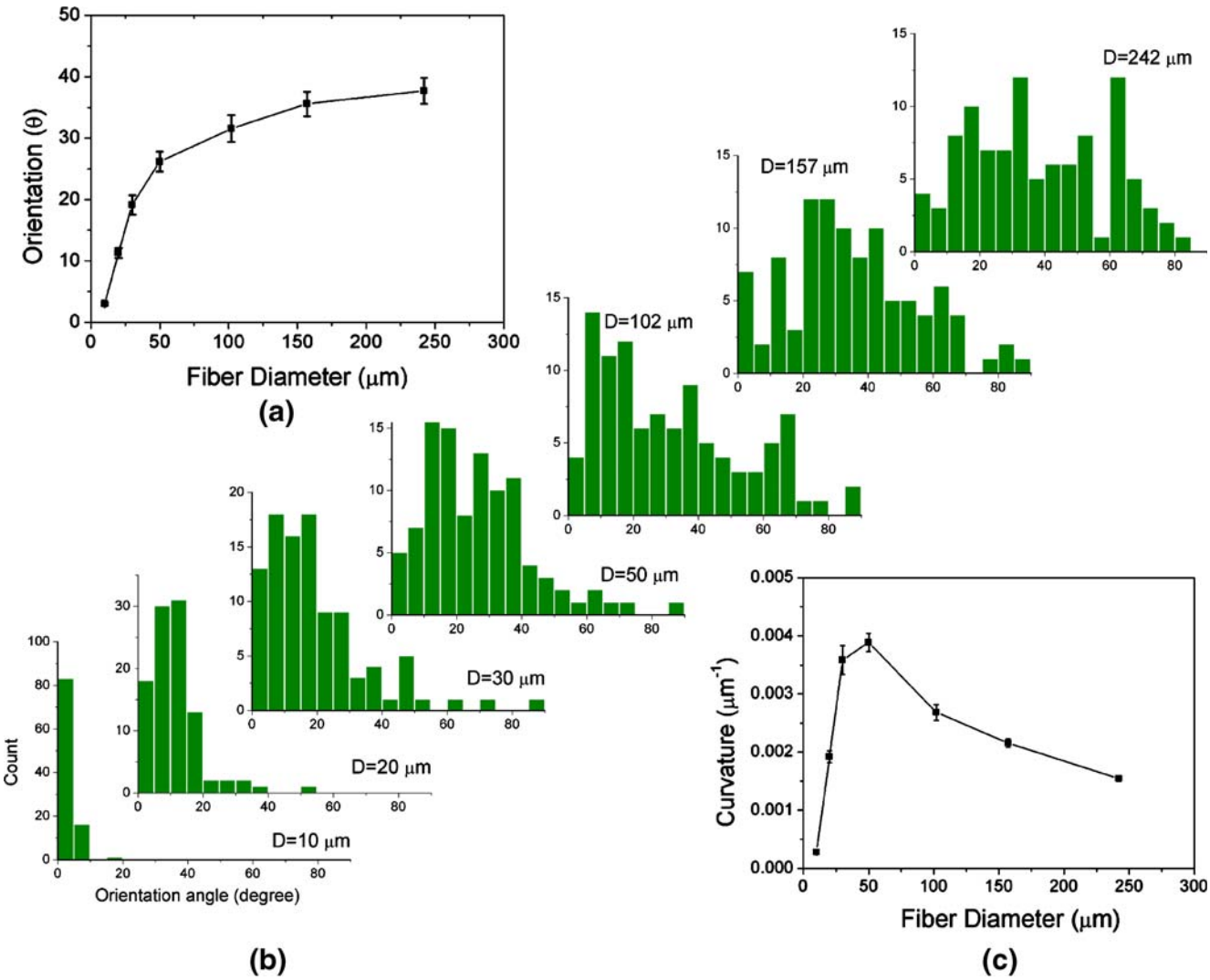

Fig. 4 Quantification of cellular alignment on PLGA microfibers. (**a**) Orientation of cells along the fiber long axis (mean±SE). (**b**) Histogram showing the orientation distribution for each condition, normal distribution curves are overlaid on the histogram. (**c**) Cell curvature for each fiber diameter. (n=100 each)

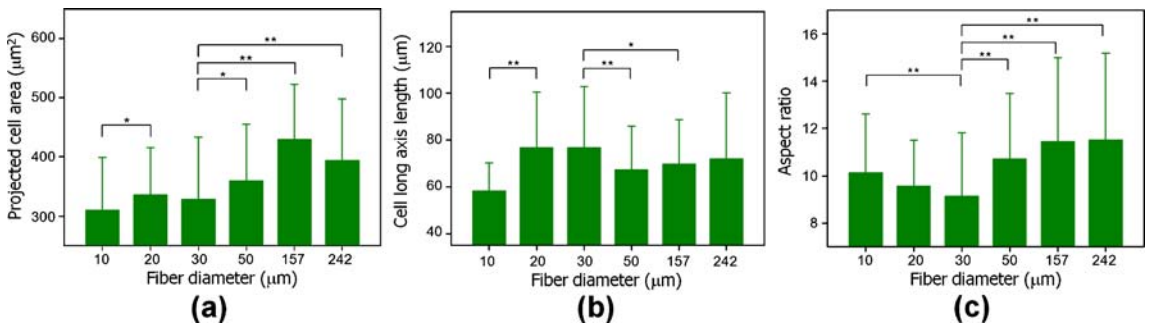

Fig. 5 Cell alignment and morphology of L929 cells on PLGA fibers, (**a**) projected cell area, (**b**) projected cell length and (**c**) aspect ratio of cells (cell length/cell width). (n=100 each, *p<0.05, **p<0.01)

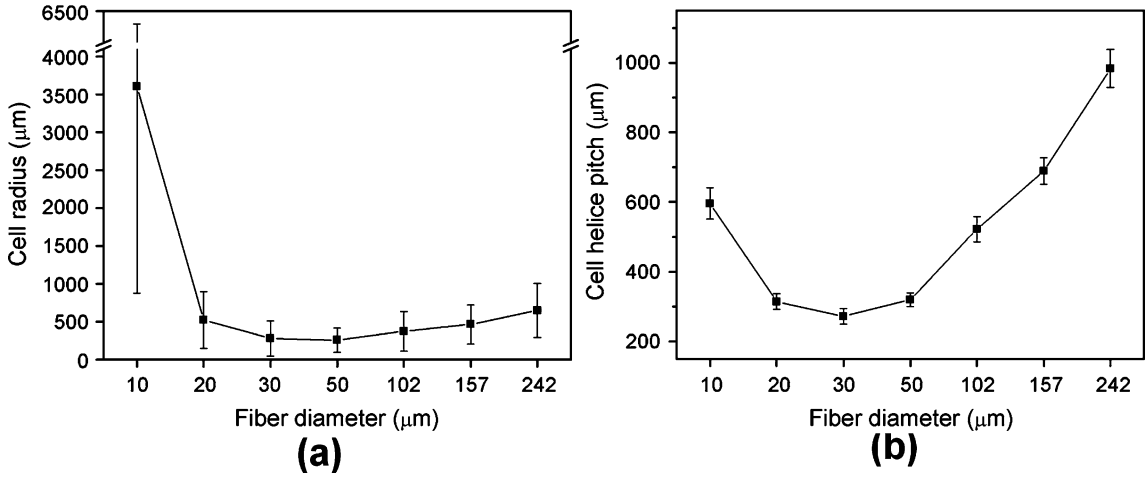

Fig. 6 Calculated values of (**a**) cell radius (mean±SD) and (**b**) pitch of cells along the cell helices (mean±SD) on PLGA fibers. (n=100 each)

fiber substrate diameter. In this study, we report that the orientation of fibroblasts increase differently as a function of fiber diameter from those of neurites.

As shown in Figs. 3 and 4, cell orientations on fibers that were 10 μm diameter did not show significant difference with fiber alignment, which is similar to the results that fibroblasts on micro- and nano-fibers aligned with fiber direction (Tian et al. 2008).

3.3 Role of focal adhesion on cell orientation

As shown in Fig. 3, fibroblasts on PLGA surfaces had elongated actin filaments with focal adhesion in the apices and peripheral region of the cell (yellow region). In these focal adhesion regions, the actin cytoskeletons are usually connected to vinculin, which binds to integrins. Cells may sense the fibrous substrates as curved surfaces, and show focal contact of vinculin and actin filament as shown by the fluorescence near the apical and peripheral region of cells, which are similar to microgrooved surfaces (Walboomers et al. 1998, 1999; Teixeira et al. 2003; Mwenifumbo et al. 2007; Tymchenko et al. 2007).

The anisotropy of cell adhesive microenvironment governs cell internal organization and orientation of polarity (Thery et al. 2006). This is controlled by focal adhesions that mediates the regulatory effects of ECM adhesion on the PLGA fibers (Pathak et al. 2007), and the variation of actin-myosin stress fibers distribution in response to the geometry of the adhesive environment (Thery et al. 2005; Pathak et al. 2007). In cell alignment on patterned substrates, focal adhesion plays an important role in fibroblast orientation, and the alignment between focal adhesion and microfilament has been observed in fibroblasts (Matsuzaka et al. 2000), macrophages and corneal epithelial cells (Britland and McCaig 1996; Teixeira et al. 2003). It is well known that when cells are cultured on microgrooved or micropatterned surfaces, the focal adhesion proteins such as actin and vinculin condensates along the ridges of substrates in various cell types (Wojciak-Stothard et al. 1995; Oakley et al. 1997; Walboomers et al. 1999). Although the reason of this phenomenon is not fully understood, it is suggested that the biochemomechanical signals, environmental and internal cellular mechanisms (Pathak et al. 2007; Wei et al. 2008), may play a role in this behavior.

There may also possibilities of other factors affecting cell orientations such as surface nanotopography or ECM components. To reduce the effect of ECM, the samples were not treated with any adhesive coatings or pretreatments. The PLGA fibers used in this study did not have completely smooth surfaces and contained small (<1 μm) wrinkles that could be observed by SEM. But, in comparison to the other environmental factors, major factor that varied in our samples was the curvature of cell substrates.

3.4 Controlled cell microenvironments

The cell morphologies in tissue constructs provide organ specific mechanical, physiological functions. These cell morphologies can be adjusted by 3D microenvironments in tissue engineering technologies. Micro-controlled scaffolds are potent choice to define cell morphologies, mechanical strength, and even differentiation of stem cells with incorporation of appropriate growth factors.

Although fibroblasts have tissue specific gene-expression profiles and synthesize ECM proteins and secrete cytokines in a site-specific manner (Chang et al. 2002), fibroblasts from different anatomical sites have similar morphology. Therefore the ability to control the orientation of fibroblasts may be applied to various tissue regenerative fields, where fibroblasts are included one

component of the tissues. By controlling the curvature or morphologies in scaffold designing stages, the defined tissue orientation and textures can be achieved simple manner. This scaffold microscopic feature designing can be a potent factor for tailored cell alignment and may be an important contributor for controlling tissue architecture of desired part of organs in clinical applications.

4 Conclusion

In this study, mouse fibroblast L929 fibroblasts cultured on different diameter PLGA fibrous substrate showed preferred orientation angles and curvatures. Fibroblastic cells exhibited increasing orientation angle with respect to long axis of PLGA fiber substrates as the diameter increases. Using this property, it was possible to control the orientation angles by changing the fiber diameter from ten to several hundred micrometers.

The control of orientation may be applicable to tailored design of microstructured tissues. There are many potential applications in regenerative medicine and tissue engineering in human tissue rehabilitations, for example, ligament, tendon, muscle and nerve bundles. Fibrous scaffolds functionalized with controlling cell orientation have potentials to contribute to clinical application for replacing and reconstructing diseased and injured tissues.

Acknowledgements This study was supported by a grant from the Korea Health 21 R&D Project, Ministry for Health, Welfare and Family Affairs (0405-ER01-0304-0001), and the National Research Lab (NRL) program, the Korea Science and Engineering Foundation (KOSEF; R0A-2007-000-20086-0), Republic of Korea.

References

C.A. Bashur, L.A. Dahlgren, A.S. Goldstein, Biomaterials **27**(33), 5681–5688 (2006). doi:10.1016/j.biomaterials.2006.07.005

C.J. Bettinger, B. Orrick, A. Misra, R. Langer, J.T. Borenstein, Biomaterials **27**(12), 2558–2565 (2006). doi:10.1016/j.biomaterials.2005.11.029

S. Britland, C. McCaig, Exp. Cell Res. **226**(1), 31–38 (1996). doi:10.1006/excr.1996.0199

H.Y. Chang, J.T. Chi, S. Dudoit, C. Bondre, M. van de Rijn, D. Botstein, P.O. Brown, Proc. Natl. Acad. Sci. U. S. A. **99**(20), 12877–12882 (2002). doi:10.1073/pnas.162488599

S.Y. Chew, R. Mi, A. Hoke, K.W. Leong, Biomaterials **29**(6), 653–661 (2008). doi:10.1016/j.biomaterials.2007.10.025

C.H. Choi, S.H. Hagvall, B.M. Wu, J.C. Dunn, R.E. Beygui, C.J. Kim, Biomaterials **28**(9), 1672–1679 (2007). doi:10.1016/j.biomaterials.2006.11.031

G.A. Dunn, J.P. Heath, Exp. Cell Res **101**(1), 1–14 (1976). doi:10.1016/0014-4827(76)90405-5

C.M. Hwang, A. Khademhosseini, Y. Park, K. Sun, S.H. Lee, Langmuir **24**(13), 6845–6851 (2008). doi:10.1021/la800253b

W. Jeong, J. Kim, S. Kim, S. Lee, G. Mensing, D.J. Beebe, Lab. Chip **4**(6), 576–580 (2004). doi:10.1039/b411249k

W.J. Jeong, J.Y. Kim, J. Choo, E.K. Lee, C.S. Han, D.J. Beebe, G.H. Seong, S.H. Lee, Langmuir **21**(9), 3738–3741 (2005). doi:10.1021/la0501051

A. Khademhosseini, R. Langer, J. Borenstein, J.P. Vacanti, Proc. Natl. Acad. Sci. U. S. A. **103**(8), 2480–2487 (2006). doi:10.1073/pnas.0507681102

S. Kim, H. Oh, J. Baek, H. Kim, W. Kim, S. Lee, Lab. Chip **5**(10), 1168–1172 (2005). doi:10.1039/b506194f

N. L'Heureux, N. Dusserre, G. Konig, B. Victor, P. Keire, T.N. Wight, N.A. Chronos, A.E. Kyles, C.R. Gregory, G. Hoyt, R.C. Robbins, T.N. McAllister, Nat. Med **12**(3), 361–365 (2006). doi:10.1038/nm1364

C.H. Lee, H.J. Shin, I.H. Cho, Y.M. Kang, I.A. Kim, K.D. Park, J.W. Shin, Biomaterials **26**(11), 1261–1270 (2005). doi:10.1016/j.biomaterials.2004.04.037

J. Mai, C. Sun, S. Li, X. Zhang, Biomed. Microdevices **9**(4), 523–531 (2007). doi:10.1007/s10544-007-9060-8

K. Matsuzaka, F. Walboomers, A. de Ruijter, J.A. Jansen, Clin. Oral Implants Res. **11**(4), 325–333 (2000). doi:10.1034/j.1600-0501.2000.011004325.x

T.K. Monsees, K. Barth, S. Tippelt, K. Heidel, A. Gorbunov, W. Pompe, R.H. Funk, Cells Tissues Organs **180**(2), 81–95 (2005). doi:10.1159/000086749

R. Murugan, S. Ramakrishna, Tissue Eng. **13**(8), 1845–1866 (2007). doi:10.1089/ten.2006.0078

S. Mwenifumbo, M. Li, J. Chen, A. Beye, W. Soboyejo, J. Mater. Sci. Mater. Med. **18**(1), 9–23 (2007). doi:10.1007/s10856-006-0658-9

T. Neumann, S.D. Hauschka, J.E. Sanders, Tissue Eng. **9**(5), 995–1003 (2003). doi:10.1089/107632703322495637

C. Oakley, N.A. Jaeger, D.M. Brunette, Exp. Cell Res. **234**(2), 413–424 (1997). doi:10.1006/excr.1997.3625

H.J. Oh, S.H. Kim, J.Y. Baek, G.H. Seong, S.H. Lee, J. Micromech. Microeng **16**(2), 285–291 (2006). doi:10.1088/0960-1317/16/2/013

P.T. Ohara, R.C. Buck, Exp. Cell Res. **121**(2), 235–249 (1979). doi:10.1016/0014-4827(79)90002-8

A. Pathak, V.S. Deshpande, R.M. McMeeking, A.G. Evans, J. R. Soc. Interface **5**, 507–524 (2007)

R.M. Smeal, R. Rabbitt, R. Biran, P.A. Tresco, Ann. Biomed. Eng. **33**(3), 376–382 (2005)

A.I. Teixeira, G.A. Abrams, P.J. Bertics, C.J. Murphy, P.F. Nealey, J. Cell. Sci. **116**(Pt 10), 1881–1892 (2003)

M. Thery, V. Racine, A. Pepin, M. Piel, Y. Chen, J.B. Sibarita, M. Bornens, Nat. Cell. Biol. **7**(10), 947–953 (2005)

M. Thery, V. Racine, M. Piel, A. Pepin, A. Dimitrov, Y. Chen, J.B. Sibarita, M. Bornens, Proc. Natl. Acad. Sci. U. S. A. **103**(52), 19771–19776 (2006)

F. Tian, H. Hosseinkhani, M. Hosseinkhani, A. Khademhosseini, Y. Yokoyama, G.G. Estrada, H. Kobayashi, J. Biomed. Mater. Res. **84A**, 291–299 (2008)

N. Tymchenko, J. Wallentin, S. Petronis, L.M. Bjursten, B. Kasemo, J. Gold, Biophys J **93**(1), 335–345 (2007)

X.F. Walboomers, H.J. Croes, L.A. Ginsel, J.A. Jansen, Biomaterials **19**(20), 1861–1868 (1998)

X.F. Walboomers, W. Monaghan, A.S. Curtis, J.A. Jansen, J. Biomed. Mater. Res. **46**(2), 212–220 (1999)

Z. Wei, V.S. Deshpande, R.M. McMeeking, A.G. Evans, J. Biomech. Eng **130**(3), 031009 (2008)

E.W. Weisstein, Helix. MathWorld–A Wolfram Web Resource. (2008) http://mathworld.wolfram.com/Helix.html Accessed Oct 22 2008

B. Wojciak-Stothard, Z. Madeja, W. Korohoda, A. Curtis, C. Wilkinson, Cell. Biol. Int. **19**(6), 485–490 (1995)

T. Wong, J.A. McGrath, H. Navsaria, Br J Dermatol **156**(6), 1149–1155 (2007)

S. Yamamoto, M. Tanaka, H. Sunami, E. Ito, S. Yamashita, Y. Morita, M. Shimomura, Langmuir **23**(15), 8114–8120 (2007)